AEROSPACE REPORT NO..
TR-0090(5940-06)-6

Observations of Correlated Broadband Electrostatic Noise and Electron Cyclotron Emissions in the Plasma Sheet

Prepared by

J. L. Roeder
Space Sciences Laboratory
Laboratory Operations

V. Angelopoulos
Department of Physics
University of California
Los Angeles, CA

W. Baumjohann
Max–Planck Institute for Physics and Astrophysics
Federal Republic of Germany

and

R. R. Anderson
Department of Physics and Astronomy
University of Iowa
Iowa City, IA

15 January 1991

Prepared for

SPACE SYSTEMS DIVISION
AIR FORCE SYSTEMS COMMAND
Los Angeles Air Force Base
P.O. Box 92960
Los Angeles, CA 90009-2960

Engineering and Technology Group

*Original contains color
plates: All DTIC reproduct-
ions will be in black and
white*

THE AEROSPACE CORPORATION
El Segundo, California

DTIC
ELECTE
FEB 20 1991

AD-A231 660

91 2 20 007

This report was submitted by The Aerospace Corporation, El Segundo, CA 90245, under Contract No. F04701-88-C-0089 with the Space Systems Division, P. O. Box 92960, Los Angeles, CA 90009-2960. It was reviewed and approved for The Aerospace Corporation by A. B. Christensen, Director, Space Sciences Laboratory. Lt Tyron Fisher was the project officer for the Mission–Oriented Investigation and Experimentation (MOIE) Program.

This report has been reviewed by the Public Affairs Office (PAS) and is releasable to the National Technical Information Service (NTIS). At NTIS, it will be available to the general public, including foreign nationals.

This technical report has been reviewed and is approved for publication. Publication of this report does not constitute Air Force approval of the report's findings or conclusions. It is published only for the exchange and stimulation of ideas.

TYRON FISHER, Lt, USAF
MOIE Project Officer
SSD/CLPO

JONATHAN M. EMMES, Maj, USAF
MOIE Program Manager
AFSTC/WCO OL-AB

REPORT DOCUMENTATION PAGE

1a. REPORT SECURITY CLASSIFICATION Unclassified		1b. RESTRICTIVE MARKINGS
2a. SECURITY CLASSIFICATION AUTHORITY		3. DISTRIBUTION/AVAILABILITY OF REPORT Approved for public release; distribution unlimited
2b. DECLASSIFICATION/DOWNGRADING SCHEDULE		
4. PERFORMING ORGANIZATION REPORT NUMBER(S) TR-0090(5940-06)-6		5. MONITORING ORGANIZATION REPORT NUMBER(S) SSD-TR-91-01

6a. NAME OF PERFORMING ORGANIZATION The Aerospace Corporation Laboratory Operations	6b. OFFICE SYMBOL (If applicable)	7a. NAME OF MONITORING ORGANIZATION Space Systems Division
6c. ADDRESS (City, State, and ZIP Code) El Segundo, CA 90245-4691		7b. ADDRESS (City, State, and ZIP Code) Los Angeles Air Force Base Los Angeles, CA 90009-2960
8a. NAME OF FUNDING/SPONSORING ORGANIZATION	8b. OFFICE SYMBOL (If applicable)	9. PROCUREMENT INSTRUMENT IDENTIFICATION NUMBER F04701-88-C-0089

8c. ADDRESS (City, State, and ZIP Code)	10. SOURCE OF FUNDING NUMBERS			
	PROGRAM ELEMENT NO.	PROJECT NO.	TASK NO.	WORK UNIT ACCESSION NO.

11. TITLE *(Include Security Classification)*
Observations of Correlated Broadband Electrostatic Noise and Electron Cyclotron Emissions in the Plasma Sheet

12. PERSONAL AUTHOR(S) Roeder, J. L. (The Aerospace Corporation); Angelopoulos, V. (University of California); Baumjohann, W. (Max-Planck Institute for Physics and Astrophysics): and Anderson, R.R. (University of Iowa)

13a. TYPE OF REPORT	13b. TIME COVERED FROM _____ TO _____	14. DATE OF REPORT (Year, Month, Day) 1991 January 1	15. PAGE COUNT 17

16. SUPPLEMENTARY NOTATION

17. COSATI CODES			18. SUBJECT TERMS (Continue on reverse if necessary and identify by block number)
FIELD	GROUP	SUB-GROUP	Plasma sheet Plasma waves

19. ABSTRACT (Continue on reverse if necessary and identify by block number)

Electric field wave observations in the central plasma sheet show the correlated occurrence of broadband electrostatic noise and electrostatic electron cyclotron harmonic emissions. A model is proposed in which the broadband emissions are electron acoustic waves generated by an observed low energy electron beam, and the cyclotron emissions are generated by the hot electron loss cone instability. The high degree of correlation between the two emissions is provided in the model by the presence of the cold electron beam population, which allows both of the plasma instabilities to grow.

20. DISTRIBUTION/AVAILABILITY OF ABSTRACT ☐ UNCLASSIFIED/UNLIMITED ☒ SAME AS RPT. ☐ DTIC USERS	21. ABSTRACT SECURITY CLASSIFICATION Unclassified
22a. NAME OF RESPONSIBLE INDIVIDUAL	22b. TELEPHONE (Include Area Code) 22c. OFFICE SYMBOL

DD FORM 1473, 84 MAR 83 APR edition may be used until exhausted.
All other editions are obsolete

PREFACE

CONTENTS

FIGURES

I. INTRODUCTION

The electrostatic plasma wave emissions which have been detected in the Earth's magnetotail include broadband electrostatic noise and electron cyclotron emissions. These two types of waves were observed previously to be uncorrelated with one another, and they were assumed to be generated by two separate and unrelated processes. In this report, we present several observations by the AMPTE Ion Release Module (IRM) of broadband electrostatic noise and cyclotron emissions which exhibit a high degree of correlation in time. An explanation of the generation of both emissions is presented which involves an indirect link between two plasma instabilities.

Broadband electrostatic noise (BEN) emissions are impulsive electric field variations over a very wide range of frequency [*Gurnett et al.*, 1976]. Within the plasma sheet boundary layer, BEN emissions have been observed to correlate with the occurrence of ion beams, and many theories attempt to explain the wave generation by various ion beam instabilities [*Schriver and Ashour-Abdalla*, 1987]. But there are also intervals in which BEN emissions have been observed without ion beams [*Parks et al.*, 1984]. *Schriver and Ashour-Abdalla* [1989] suggested that the waves during these periods were generated by field-aligned currents carried by cold electron beams.

Narrowband electric field emissions in the harmonic bands above the local electron cyclotron frequency have also been observed in the magnetosphere. These "n + 1/2," or electron cyclotron harmonic (ECH) emissions, have been detected in the near-Earth plasma sheet [*Roeder and Koons*, 1989] and in the more distant tail regions [*Gurnett et al.*, 1976]. These emissions have been attributed to instabilities involving a positive perpendicular gradient in the hot electron velocity distribution, such as a loss cone [*Ashour-Abdalla and Kennel*, 1978].

II. OBSERVATIONS

Four months of IRM data were examined using 1-h spectrograms to find cases of correlated BEN and ECH waves. Four intervals were found in which such emissions were observed for more than 5 min. All of the cases occurred in the recovery phase of substorms, when the spacecraft was in the central plasma sheet. One example has been analyzed in detail, which occurred during a moderate substorm on April 12, 1986. The IRM was in the postmidnight sector at a radial distance of 11 to 14 R_e.

The electric field emissions observed on April 12, 1986, are shown in Figure 1 as a spectrogram of 12-s averages from the Aerospace Stepped Frequency Receiver (SFR). The figure is partitioned into three panels, with the linear frequency scales of 0.2 to 2.6 kHz, 0.9 to 9.0 kHz, and 9 to 99 kHz, respectively. The frequency ranges of the middle and bottom panels overlap so that many features are displayed twice in the spectrogram. The lines in the lower panels mark the local electron cyclotron frequency f_{ce}.

An analysis of the plasma and magnetic field data showed that the spacecraft was in the magnetotail lobe at the beginning of the contact. Several encounters with the plasma sheet boundary layer were noted in the interval 0200–0210 UT. Near 0210 UT, the IRM entered the central plasma sheet and remained in that region until the end of the pass at 0500 UT. Bursts of impulsive, broadband emissions were detected in the frequency range 0.2–10 kHz, when the plasma sheet boundary layer was encountered in the interval 0200–0210 UT. After entering the central plasma sheet at 0215 UT, the receiver continued to observe intense broadband emissions continuously until 0325 UT and sporadically thereafter. Enhancements of the electric field spectrum were also observed at frequencies near 1.2 to 1.3 f_{ce}. The occurrence of these peaks near f_{ce} was correlated with the simultaneous occurrence of the impulsive broadband emissions.

Figure 2 presents the electric field spectrum from the SFR and the University of Iowa 16-channel ELF/MF instrument during one of the most intense bursts of waves. The BEN emission was measured to be a broad enhancement from approximately 30 Hz to 10 kHz. The enhancement just above f_{ce} is clearly visible in this spectrum. If this peak is deleted from the spectrum, the remaining broadband emission has a total integrated amplitude of 0.1 mV/m. The ECH feature itself has an amplitude of 0.15 mV/m, a center frequency of 1.25 f_{ce}, and a relative bandwidth of 18%, consistent with previously observed ECH wave emissions [Roeder and Koons, 1989].

A polarization analysis was also performed on the electric field data by sorting the data into bins according to the angle between the dipole antenna and the measured magnetic field. The angular coverage by the antenna (15–90°) was sufficient to show that the broadband impulsive emissions were aligned parallel to the magnetic field, and the cyclotron emissions were polarized perpendicular to the magnetic field. This result lends credence to the interpretation that the narrowband enhancement above f_{ce} was a cyclotron wave mode and not just enhanced growth of the broadband emissions in a limited frequency range. The time series of the 10-s average amplitudes of both emissions were computed by integrating suitably edited spectra. An analysis of these series
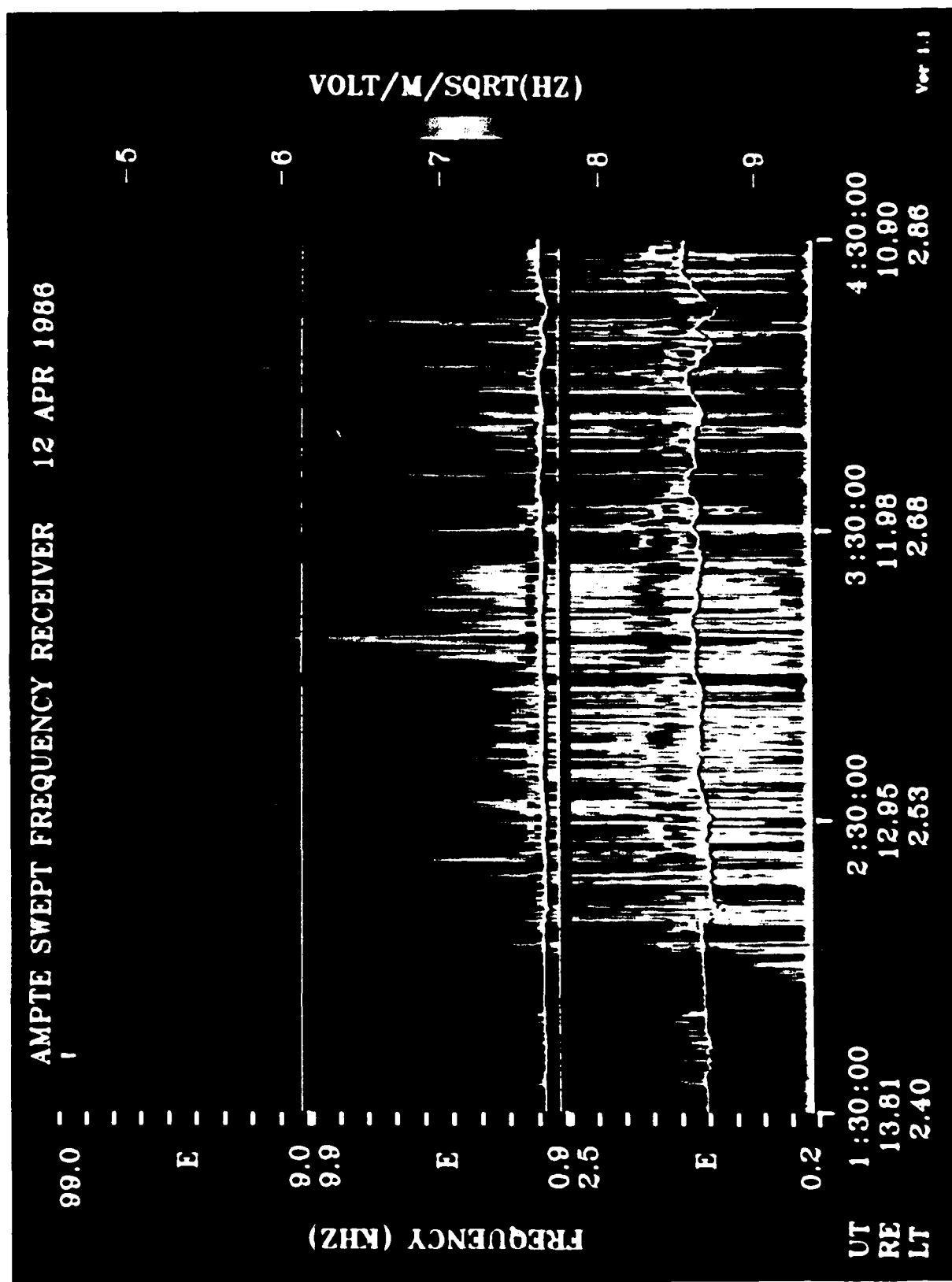
Figure 1. Spectrogram of the electric field spectral density.
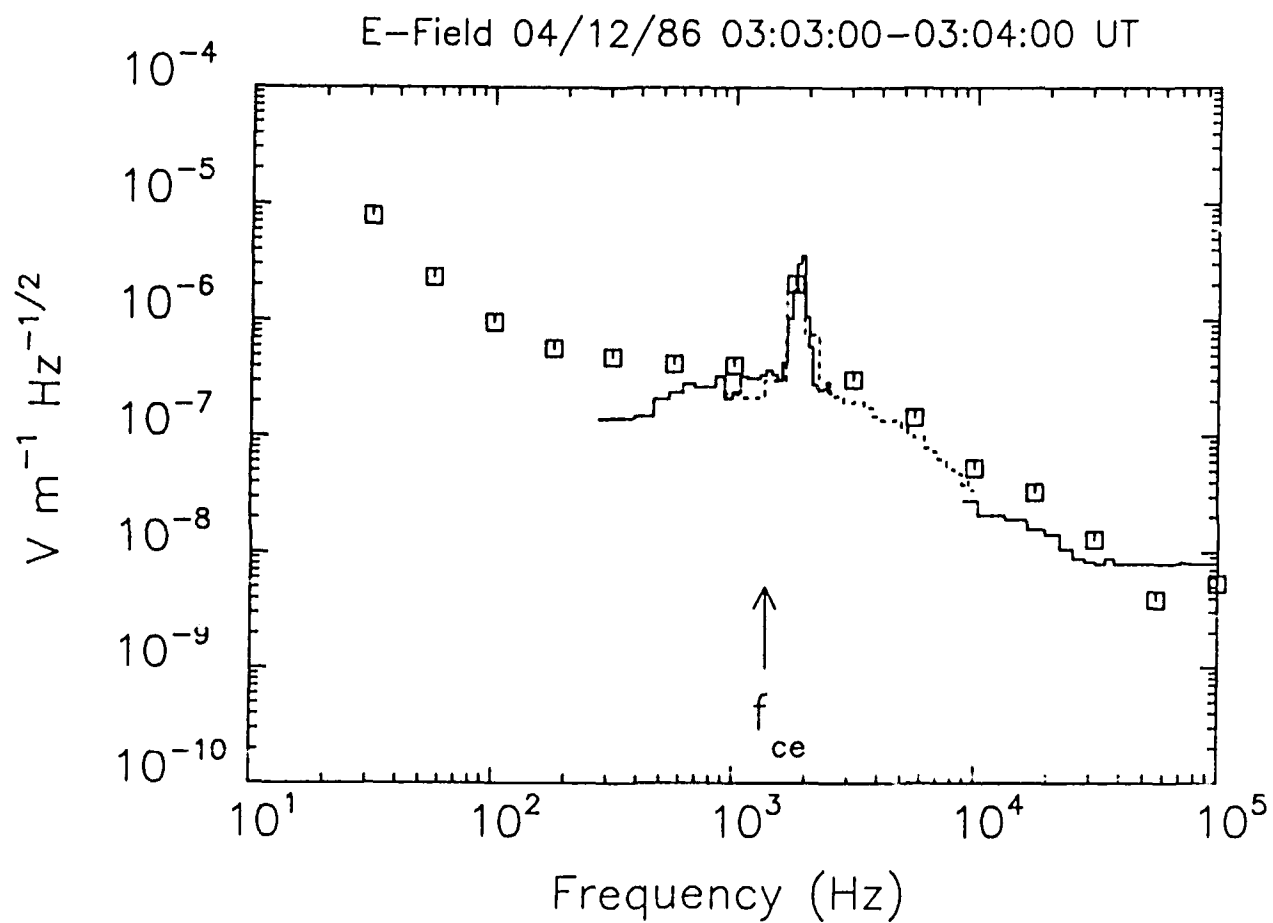
Figure 2. Electric field spectrum averaged over 60 s during the broadband and cyclotron emissions.

revealed a peak in the cross correlation function of 0.43 at a time lag of 20 to 30 s with the BEN emission occurring first. Several intervals in the data appeared to have a one-to-one correspondence between bursts of the two emissions, but the intensities of the bursts seemed unrelated.

The particle distributions observed during the BEN and ECH emissions were typical of the central plasma sheet [*Baumjohann et al.*, 1989]. No ion beams were observed in the energy range of the instrument (0.02–40 keV). The higher energy electron and ion measurements are well represented by nearly isotropic Maxwellians with densities and temperatures of $n_h \approx 0.3 \text{ cm}^{-3}$, $Th \approx 400–500$ eV, and $n_i \approx n_h$, $T_i \approx 3.5–4.3$ keV, respectively. In the range 0.020–0.060 keV, the electron distribution is uncertain because the data are contaminated by photoelectrons; however, we believe that a pronounced field aligned anisotropy at these energies provides circumstantial evidence of cold electron beams streaming upward, presumably from the ionosphere. These cold beam electrons are best fitted to a Maxwellian of density $n_c \approx 0.01 \text{ cm}^{-3}$, $T_h \approx 1$ eV, and a field-aligned bulk velocity $U_c \approx 1000$ km/s. Due to the uncertainty of the photoelectrons and the coarse energy resolution of the measurement, these values are upper limits on the beam population. The higher energy electron data showed a small temperature anisotropy, but the angular resolution of the plasma instrument is too coarse to observe the loss cone.

The observations show that the AMPTE IRM detected time correlated BEN and ECH wave emissions in the central plasma sheet for over an hour. The BEN emissions were polarized predominantly parallel to the static magnetic field, and the ECH emissions exhibited near perpendicular polarization. No ion beams were observed, but electron beams were detected streaming upward along the magnetic field at low energies.

III. LINEAR THEORY

To explain the generation of the waves, the observed plasma was modeled by a three-component Maxwellian distribution, in which a cold electron beam drifts along the magnetic field with a velocity U_c relative to a stationary hot background plasma. The density n_s and temperature T_s (thermal speed u_s) of each component were chosen to be consistent with the plasma data, where the subscript $s = c, h, i$ denotes the cold beam electrons, the hot background electrons, and the background ions, respectively. The parameters are restricted by $T_i \simeq T_h$, $T_c << T_h$, $n_c < n_h$, with the total density $n_t = n_i = n_h + n_c$, and $U_c \leq u_h$. The analysis assumes that the wave frequency is above $(\Omega_{ce}\Omega_{pi})^{1/2}$.

The two component electron distribution makes the electron acoustic instability a natural candidate for the wave generation. If the cold electron component is a beam drifting relative to the hot component, the slow electron acoustic mode may grow due to a resonance with the negative slope of the ions and/or the hot electrons at the expense of the beam kinetic energy. To investigate the generation of the ECH waves by this process, we include a magnetic field ($\Omega_{ce} < \Omega_{pe}$). Its presence is found to distort the dispersion and reduce the growth rate of the oblique electron acoustic modes.

Figure 3 summarizes a numerical study of the magnetized electrostatic plasma dispersion relation. The values of the plasma parameters are $n_c/n_{tot} = 0.05$, $T_c/T_h = 2 \times 10{-}3$, and $\Omega_{ce}\Omega_{pe} = 0.25$. The envelopes of the maximum growth rate are shown for all growing modes at all wavenumber vectors (irrespective of the branch where the growth occurs). Each curve is labeled with its value of the beam drift speed. The high frequency peaks correspond to the electron acoustic instability driven by the hot electrons, and the low frequency peaks, to the ion-driven instability. The dashed curve corresponds to the same parameters as the solid curve of $U_c = 1.25 u_h$, but it is run for $\Omega_{ce} = 0$ and is shown for comparison with the magnetized case. At the observed beam velocity of $0.1 u_h$, the high-frequency, hot-electron-driven instability is stabilized, and the growth of the ion/ion instability is nonzero only near $0.02 \Omega_{pe}$. This is a significant discrepancy between the theory and the observed wave spectrum, implying the need for a more elaborate model.

The smooth growth rates of the electron acoustic instability could possibly explain the BEN waves but cannot account for the ECH emissions. If we assume that the electron beam was the free energy source of the BEN waves, then it must have some significance in the generation of the ECH emissions since the two types of waves exhibit a high degree of correlation. ECH wave generation by an electron beam has been observed in laboratory plasmas [Seidl, 1970], but this mechanism cannot reproduce our observations for the following reasons. First, the ECH modes of the hot electrons are severely damped at large wavenumbers (i.e., for $k_\perp > \rho_h^{-1}$), unless one assumes almost perpendicular propagation. This gives a lower limit for the beam velocity required to excite the first harmonic mode: (U_c)min $> \omega/k \approx \Omega_{ce}/k_\parallel >> u_h$, which is large compared to our observations. This is corroborated by Figure 3, where for a beam velocity as high as $1.25 u_h$ there is no
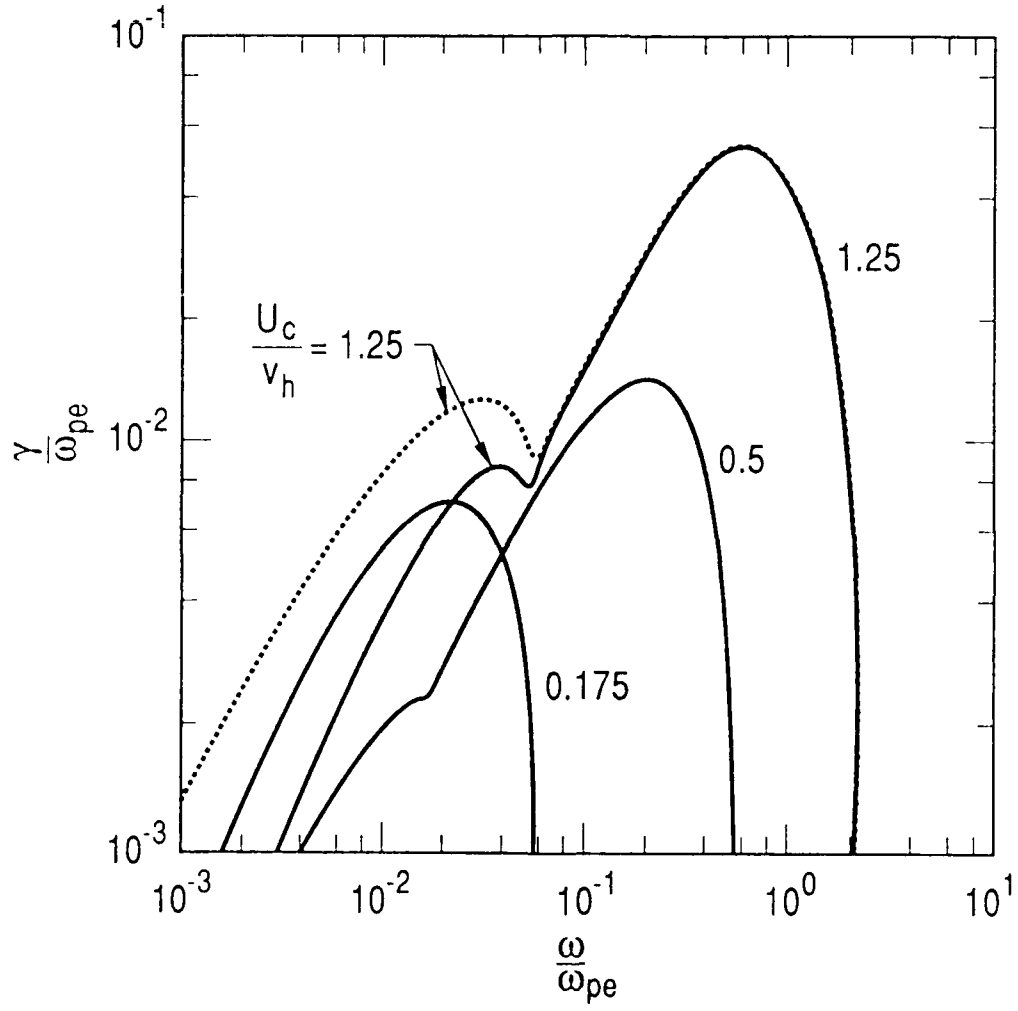
Figure 3. Temporal growth rate envelopes of all growing modes at all wave numbers and angles of propagation for several beam velocities.

peak near the cyclotron frequency. Second, electron beams usually generate higher harmonic emissions, yet our measurements show no second harmonic emissions.

To explain the ECH waves, one must assume a perpendicular gradient in the electron velocity distribution for a free energy source. Most theories of ECH emissions use a loss cone in the hot electron distribution. *Young* [1973] showed that a mild loss cone feature embedded on an electron distribution cannot give growth to ECH waves unless another much colder electron component is present. The presence of the cold electrons is essential to modify the wave phase velocities in order to achieve resonance with the free energy source in the hot electrons. The Doppler shift of the perpendicular ECH modes is small, so that any streaming of the cold electrons becomes irrelevant. This provides an indirect link between the two instabilities: the beam electrons generate the BEN and also provide the ECH modes that grow due to an already existing loss cone structure of the hot electrons.

The angular resolution of the IRM plasma instrument is too coarse to observe a realistic loss cone. To make plausible the generation of the ECH waves, we have determined that such a small, unobservable feature could provide enough free energy for the instability. We solved the electrostatic dispersion relation for the model plasma, relaxing the beam velocity to zero and imposing a loss cone on the hot electron velocity distribution function. The loss cone is provided by a subtracted Maxwellian [*Ashour-Abdalla and Kennel*, 1978, equation (5)], which is characterized by a "filling" parameter Δ and a "sharpness" parameter β. Figure 4 shows the results as the marginally stable Δ versus frequency for a given β. As β becomes larger, more particles have to be subtracted from the loss cone (decreasing Δ) for the unstable spectrum to remain unstable at frequencies of 1.2 to 1.3 Ω_{ce}. This shows that a sharp but almost filled-in loss cone may be responsible for the observed ECH waves.
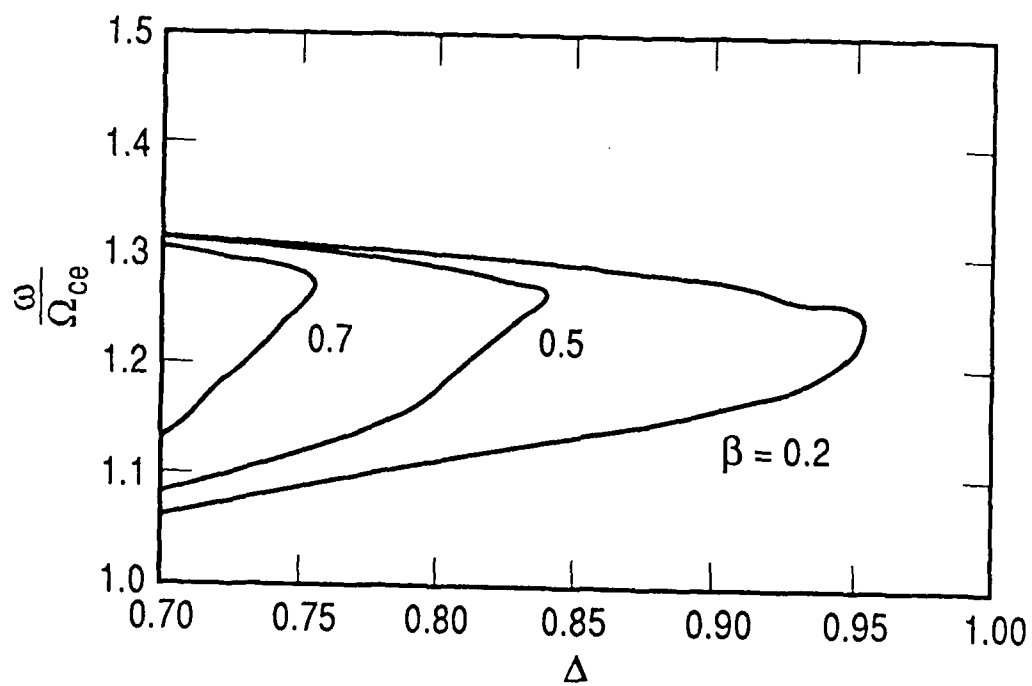
Figure 4. Marginal stability curves for the lowest frequency cold electron cyclotron mode as a function of the model parameters of the hot electron loss cone distribution.

IV. CONCLUSIONS

In a 4-month period, the AMPTE IRM observed the correlated occurrence of BEN emissions and ECH emissions in four intervals in the central plasma sheet. The measured electric field spectrum consists of a broad feature in the range 30 Hz–10 kHz and a narrowband enhancement at $1.2f_{ce}$ (2.3 kHz). These two emissions both tend to occur in bursts, with the ECH emission being detected on the trailing edge of the BEN burst. The plasma data exhibit hot particle distributions which are typical of the central plasma sheet, together with evidence of a low energy electron beam streaming upward through the hot plasma. Linear plasma theory indicates that the BEN emissions may have been generated by the beam electrons via the electron acoustic instability, although the growth of this instability is restricted to a somewhat lower frequency range than the observed wave emissions. The calculation also indicates that this process could not be the source of the ECH waves. It is proposed that the ECH emissions were generated by a loss cone instability driven by an anisotropy in the hot electron distribution which was too small to be observed by the plasma instrument. The correlation of the two emissions is due to the destabilizing action of the cold electrons on both of the instabilities.

REFERENCES

Ashour-Abdalla, M., and C. F. Kennel, "Nonconvective and convective electron cyclotron harmonic instabilities," *J. Geophys. Res.*, **83**, 1531, 1978.

Baumjohann, W., G. Paschmann, and C. A. Cattell, "Average plasma properties in the central plasma sheet," *J. Geophys. Res.*, **94**, 6597, 1989.

Gurnett, D. A., L. A. Frank, and R. P. Lepping, "Plasma waves in the magnetotail," *J. Geophys. Res.*, **81**, 6059, 1976.

Parks, G. K., M. McCarthy, R. J. Fitzenreiter, J. Etcheto, K. A. Anderson, R. R. Anderson, T. E. Eastman, L. A. Frank, D. A. Gurnett, C. Huang, R. P. Lin, A. T. Y. Lui, K. W. Ogilvie, A. Pedersen, H. Reme, and D. J. Williams, "Particle and field characteristics of the high-latitude plasma sheet boundary layer," *J. Geophys. Res.*, **89**, 8885, 1984.

Roeder, J. L., and H. C. Koons, "A survey of electron cyclotron waves in the magnetosphere and the diffuse auroral electron precipitation," *J. Geophys. Res.*, **94**, 2529, 1989.

Schriver, D., and M. Ashour-Abdalla, "Generation of high-frequency broadband electrostatic noise: the role of cold electrons," *J. Geophys. Res.*, **92**, 5807, 1987.

Schriver, D., and M. Ashour-Abdalla, "Broadband electrostatic noise due to field-aligned currents," *Geophys. Res. Lett.*, **16**, 899, 1989.

Seidl, M., "Temperature effects on high-frequency beam plasma interaction," *Phys. Fluids*, **13**, 966, 1970.

Young, T. S. T., J. D. Callen, and J. E. McCune, "High-frequency electrostatic waves in the magnetosphere," *J. Geophys. Res.*, **78**, 1082, 1973.

LABORATORY OPERATIONS

The Aerospace Corporation functions as an "architect-engineer" for national security projects, specializing in advanced military space systems. Providing research support, the corporation's Laboratory Operations conducts experimental and theoretical investigations that focus on the application of scientific and technical advances to such systems. Vital to the success of these investigations is the technical staff's wide-ranging expertise and its ability to stay current with new developments. This expertise is enhanced by a research program aimed at dealing with the many problems associated with rapidly evolving space systems. Contributing their capabilities to the research effort are these individual laboratories:

Aerophysics Laboratory: Launch vehicle and reentry fluid mechanics, heat transfer and flight dynamics; chemical and electric propulsion, propellant chemistry, chemical dynamics, environmental chemistry, trace detection; spacecraft structural mechanics, contamination, thermal and structural control; high temperature thermomechanics, gas kinetics and radiation; cw and pulsed chemical and excimer laser development, including chemical kinetics, spectroscopy, optical resonators, beam control, atmospheric propagation, laser effects and countermeasures.

Chemistry and Physics Laboratory: Atmospheric chemical reactions, atmospheric optics, light scattering, state-specific chemical reactions and radiative signatures of missile plumes, sensor out-of-field-of-view rejection, applied laser spectroscopy, laser chemistry, laser optoelectronics, solar cell physics, battery electrochemistry, space vacuum and radiation effects on materials, lubrication and surface phenomena, thermionic emission, photosensitive materials and detectors, atomic frequency standards, and environmental chemistry.

Electronics Research Laboratory: Microelectronics, solid-state device physics, compound semiconductors, radiation hardening; electro-optics, quantum electronics, solid-state lasers, optical propagation and communications; microwave semiconductor devices, microwave/millimeter wave measurements, diagnostics and radiometry, microwave/millimeter wave thermionic devices; atomic time and frequency standards; antennas, rf systems, electromagnetic propagation phenomena, space communication systems.

Materials Sciences Laboratory: Development of new materials: metals, alloys, ceramics, polymers and their composites, and new forms of carbon; nondestructive evaluation, component failure analysis and reliability; fracture mechanics and stress corrosion; analysis and evaluation of materials at cryogenic and elevated temperatures as well as in space and enemy-induced environments.

Space Sciences Laboratory: Magnetospheric, auroral and cosmic ray physics, wave-particle interactions, magnetospheric plasma waves; atmospheric and ionospheric physics, density and composition of the upper atmosphere, remote sensing using atmospheric radiation; solar physics, infrared astronomy, infrared signature analysis; effects of solar activity, magnetic storms and nuclear explosions on the earth's atmosphere, ionosphere and magnetosphere; effects of electromagnetic and particulate radiations on space systems; space instrumentation.